Contents lists available at Indonesian Scholar Society
Indonesian Journal of Data Risk Research
Journal Homepage:
https://journal.solusiriset.com/index.php/ijdrr/index
e-ISSN: xxxx-xxxx

A Hybrid SVD–Log Ratio Framework for Satellite-Based Disaster Damage Segmentation and Impact Mapping

Faris Alaudin Shalih[1], Achmad Abdurrazzaq[2*]

[1] Indonesian Army, Indonesia
[2] Department of Mathematics, Indonesia Defense University, Indonesia

Corresponding Email: achmad.abdurrazzaq@idu.ac.id

ABSTRACT

Indonesia is a region prone to various natural disasters, requiring a monitoring system capable of detecting changes in impacted areas quickly and accurately. This study proposes a method for segmenting satellite images that combines singular value decomposition and log ratio approaches to identify disaster impacts using Sentinel-2 satellite images. The segmentation process consists of preprocessing steps such as RGB to HSV colour conversion and histogram matching. The processing stage involves applying singular value decomposition on each 2×2 kernel block, where the smallest singular value is used as an indicator of local differences. This is then combined with a log operation to reduce speckle noise. The segmentation results are refined through postprocessing by overlaying satellite data to enhance the visibility of affected areas. Quantitative evaluation using ROC curves and AUC shows that this combination achieves high detection accuracy, with a maximum AUC value of 0.9216, outperforming the Otsu method (0.8123), Region Growing (0.8349), and K-Means (0.8731). This combination has proven effective in distinguishing image changes in detail and holds potential for application in an automatic, real-time disaster impact monitoring system in disaster-prone areas.

ARTICLE INFO

Received
23 Jan 2026
Revised
22 March 2026
Accepted
26 Mei 2026

Keywords: Disaster; Image Segmentation; Log-Ratio; Singular Value Decomposition.

I. INTRODUCTION

Indonesia is the world's largest archipelago, comprising 17,000 islands scattered along the equator [1], [2], [3]. Its strategic location at the junction of three major tectonic plates, the Indo-Australian Plate, the Eurasian Plate, and the Pacific Plate, makes Indonesia highly vulnerable to

various types of natural disasters [4], [5], [6]. This vulnerability is exacerbated by global climate change, which increases the frequency and intensity of natural disasters [7], [8], [9]. These events not only cause massive material losses but also result in significant loss of life and leave deep psychological impacts on survivors [10], [11], [12]. Furthermore, the impacts of natural disasters also have the potential to disrupt social, economic, and political stability at the national level, which can ultimately affect national resilience [13], [14], [15].

As the complexity of disasters and their impacts increase, the need for accurate, timely, and comprehensive data has become increasingly urgent. Satellite imagery technology offers a highly effective solution for providing widely accessible and sustainable observational data that covers vast areas and is capable of delivering visual information about on-the-ground conditions in a relatively short time [16], [17], [18], [19]. Satellite imagery can capture environmental changes before and after a disaster, providing a clear picture of the resulting impacts, and aiding in emergency response planning and recovery efforts [20], [21], [22]. Raw data from satellite imagery typically consists of a vast and complex amount of information, requiring advanced analytical methods to extract meaningful and operationally usable information [23], [24], [25].

Singular value decomposition (SVD) is a mathematical technique that can be used to analyze the data structure in satellite images by decomposing the image matrix into singular components that represent the key information in the data [26], [27], [28], [29]. Local kernels are used as an approach in the application of SVD to capture patterns of change at the pixel level by considering inter-pixel relationships within a specific area [30], [31], [32], [33]. Disaster monitoring can utilize SVD techniques to identify significant change patterns in satellite imagery related to disaster impacts. Image segmentation is another technique that can be used to divide satellite images into smaller, homogeneous segments based on specific characteristics, such as color, texture, or brightness [34], [35], [36]. The division of images into smaller segments is the fundamental concept of image segmentation, which facilitates the analysis and mapping of disaster impacts. Image segmentation can be used to identify and map areas that have suffered severe damage during a disaster. The combined use of these techniques enables a more in-depth and comprehensive analysis of disaster impacts, which can serve as the basis for more effective and efficient emergency response planning.

Based on research of [37], a target detection method for Synthetic Aperture Radar (SAR) images has been developed by combining a visual attention model and SVD. The main steps in this method involve decomposing the SAR image matrix using SVD, then reconstructing the image by retaining only a subset of the largest singular values. This process allows the system to focus on important information interpreted as segmentation targets. This aligns with the process of ignoring irrelevant background information. The results show that this method successfully detected all target areas in images with simple environments, whereas conventional methods such as the Itti-Koch model detected only about 43% of the target areas. This approach is effective for SAR images; however, the study did not yet implement a combination of local kernel-based segmentation techniques and SVD, which has the potential to improve accuracy in

the segmentation process for more complex satellite images. Further research is certainly needed to test the effectiveness of integrating SVD and local kernels.

Previous research has demonstrated the effectiveness of integrating SVD with various approaches in a range of image object detection applications. Previous research also revealed that there are still gaps in the application of combining change segmentation methods with the singular value approach in SVD for satellite image data segmentation. The application of disaster image segmentation based on a combination of the singular value and log ratio approaches is expected to provide more accurate and detailed information regarding post-disaster conditions to the government and relevant agencies in Indonesia. This information is crucial for supporting rapid and precise decision-making in emergency situations, as well as for long-term planning to enhance regional resilience. A better understanding of disaster impacts can also assist Indonesia in formulating more effective policies for future risk mitigation. These efforts are vital for reducing disaster risks, strengthening infrastructure, and improving community preparedness.

II. METHODS

1. Dataset

The data used in this study consists of multispectral satellite imagery obtained from the Sentinel-2 dataset. These satellite images were selected because they have sufficient spatial and temporal resolution for disaster impact analysis. The first dataset, the test dataset, will be downloaded from the Copernicus Open Access Hub satellite imagery provider [38]. The second dataset, the training dataset, will use the Semantic Change Detection Dataset (SECOND) [39], which consists of 200 images. The satellite imagery used covers pre- and post-disaster conditions, which are necessary for analyzing changes resulting from disasters. The downloaded data uses the RGB (Red, Green, Blue) channel, PNG format, and has dimensions of 1024×576 pixels. The disaster test data to be used is presented in Table 1.

Table 1. Research Data

No.	Disaster Data	Time of Disaster	Pre-Disaster Data	Post-Disaster Data
1	Palu Liquefaction, Indonesia	28/09/2018	19/07/2018	22/10/2018
2	Masamba Flood, Indonesia	13/07/2020	09/04/2020	28/07/2020
3	Gaza War, Palestina	19/10/2024	26/12/2021	20/01/2024

The primary variable analyzed in this study is significant changes in image pixels in pre- and post-disaster data, which can indicate disaster-related damage. Therefore, the data collected must be free from weather-related influences; as a result, for some datasets, it is necessary to collect data at sufficiently long intervals between the pre- and post-disaster periods and the actual time the disaster occurred. The data used in this study are illustrated in Figure 1.

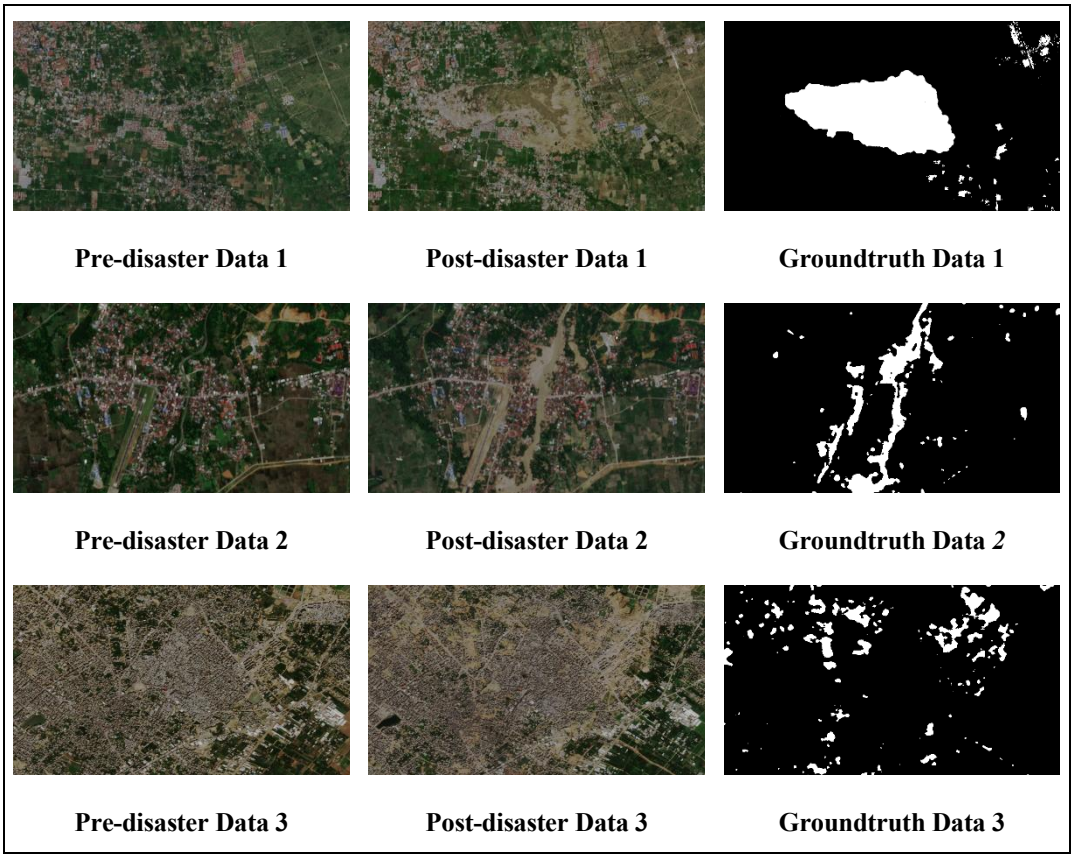

(a) Data Test

(b) Data Train

Figure 1. Image Data Used for the Experimental Purposes

2. Proposed Framework

The proposed framework consists of three main stages. The first stage is data preprocessing, which involves the initial processing of two satellite images taken from disaster events in Indonesia. The second stage is processing, which involves the application of a singular value-based segmentation method as the primary method for detecting disaster-affected areas. The third stage is

postprocessing and evaluation, which aims to assess the segmentation results and compare them with methods from previous studies.

Step 1: The preprocessing consists of two main processes: histogram matching and image conversion to the Hue-Saturation-Value (HSV) color space. This process begins by calculating the intensity histogram of each image. Next, the cumulative distribution function (CDF) is derived using Equations 1 and 2.2. Once both distribution functions are obtained, mapping is performed from the post-disaster image to the pre-disaster image using Equation 2. This alignment will assist the segmentation process carried out in the next stage so that it focuses more on spatial changes caused by the disaster, rather than being influenced by differences in intensity due to lighting or sensors. Next, the RGB image is converted to HSV to facilitate the identification of relevant areas during the segmentation process.

$$T(r_k) = \sum_{i=0}^{k} p_r(r_i) \tag{1}$$

$$G(z_k) = \sum_{i=0}^{k} p_r(z_i) \tag{2}$$

Step 2: Image processing involves two segmentation steps: (i) a singular value decomposition (SVD) operation as per Equation 3, whose output is the average of the second singular values (σ_2) for each image. Next, based on the first stage, the average of all previous second singular values (σ_2) is calculated and used as the first threshold (β_1). (ii) a log ratio operation, the output of which is the average log ratio value for each image. Next, based on the second stage, the average of all previous log ratio values is calculated and used as the second threshold (β_2).

$$A = U\Sigma V^T \tag{3}$$

Step 3: Postprocessing is the final step in image analysis, serving to refine the segmentation results and evaluate the model's accuracy in detecting disaster-affected areas. The first step is the binary thresholding process, which involves converting the pixel values from the segmentation result C_2 into binary values based on the presence of changes. Pixels with values greater than zero are converted to 1 (white), while the rest become 0 (black), as stated in Equation 4.

$$C_2(x,y) = \begin{cases} 1 & , \text{if } C_2(x,y) > 0 \\ 0 & , \text{otherwise} \end{cases} \tag{4}$$

The next step is to evaluate accuracy using the ROC-AUC approach, which involves comparing the binary segmentation results with the reference data. The segmentation results are then visualized on the original image to generate a Disaster Impact Map (DIM) that shows the areas where changes have been detected.

To better understand each stage of the proposed framework, Figure 2 provides a complete flowchart of the process.

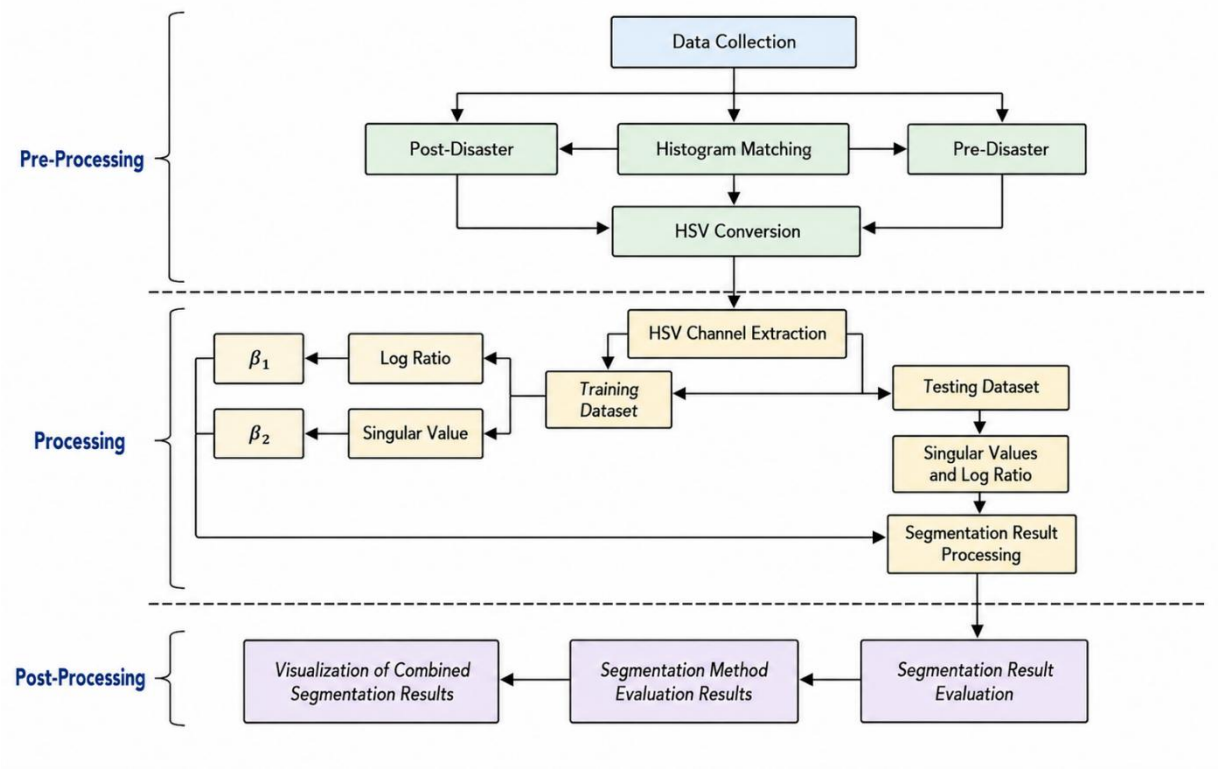

Figure 2. Flowchart of the Proposed Framework

III. RESULTS AND DISCUSSION

During the preprocessing stage, the input image in Figure 1 is converted into an HSV color space, as shown in Figure 3.

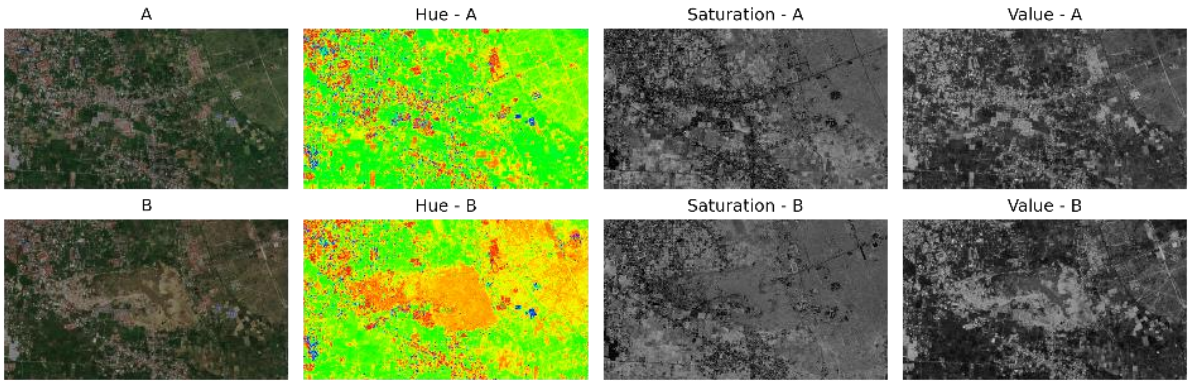

Disaster Data 1

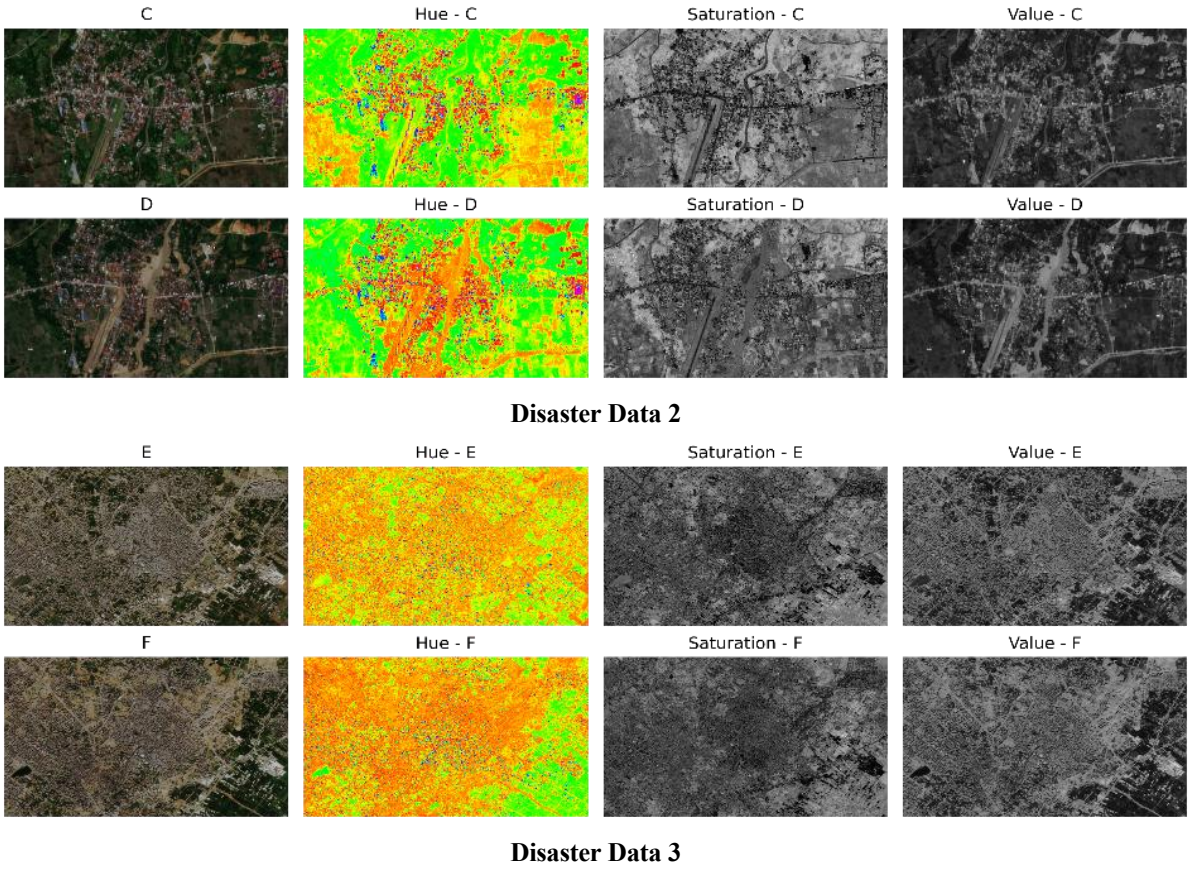

Figure 3. Image Conversion Results to the HSV Color Channel

Figure 3 shows three groups of pre-processed images from different disaster sites, labelled Disaster data 1, Disaster data 2, and Disaster data 3. These three datasets represent the unique damage characteristics of each affected area, as indicated by differences in pixel intensity. These results serve as input for the next stage, the processing stage.

In this study, singular values serve as the basis for image classification and feature extraction. The selection of singular values is based on an analysis of how singular values behave in relation to the distribution of values in matrix A.

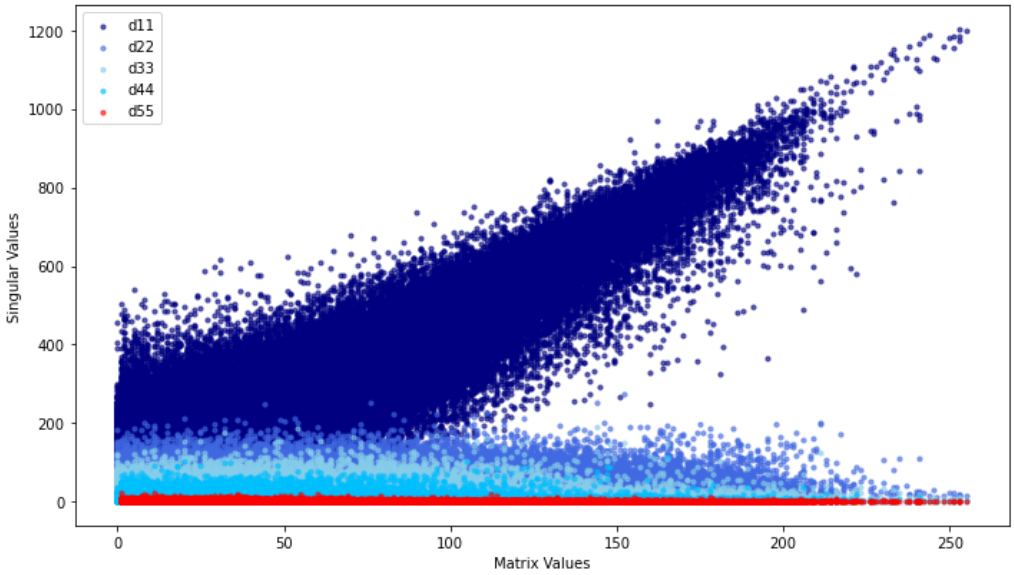

Figure 4. Distribution of the Singular Values of Matrix A

Based on Figure 4, the distribution of singular values relative to pixel value variations within the local matrix reveals significant differences in characteristics among the components. The first singular component ($d11$) exhibits a linear and consistent growth trend, indicating the dominance of stable global information across the entire image. Conversely, the last singular value (dnn), in this case $d55$, is narrowly distributed with relatively low values and minimal fluctuations. This pattern reflects high sensitivity to subtle changes around the kernel's center. The last singular value holds potential as a strong indicator in local-based segmentation due to its ability to highlight small dynamics undetected by the primary components. This approach enables more adaptive modeling of local texture and structural variations in the image. The strategy of utilizing dnn provides an opportunity for segmentation algorithms to focus on relevant features, without relying solely on the dominant information from the first singular component.

Figure 5 provides a sample to determine the relationship between the second singular value in SVD and the log ratio as a change detector for the dataset. This is done to formulate a new equation that will be used in the second stage of processing.

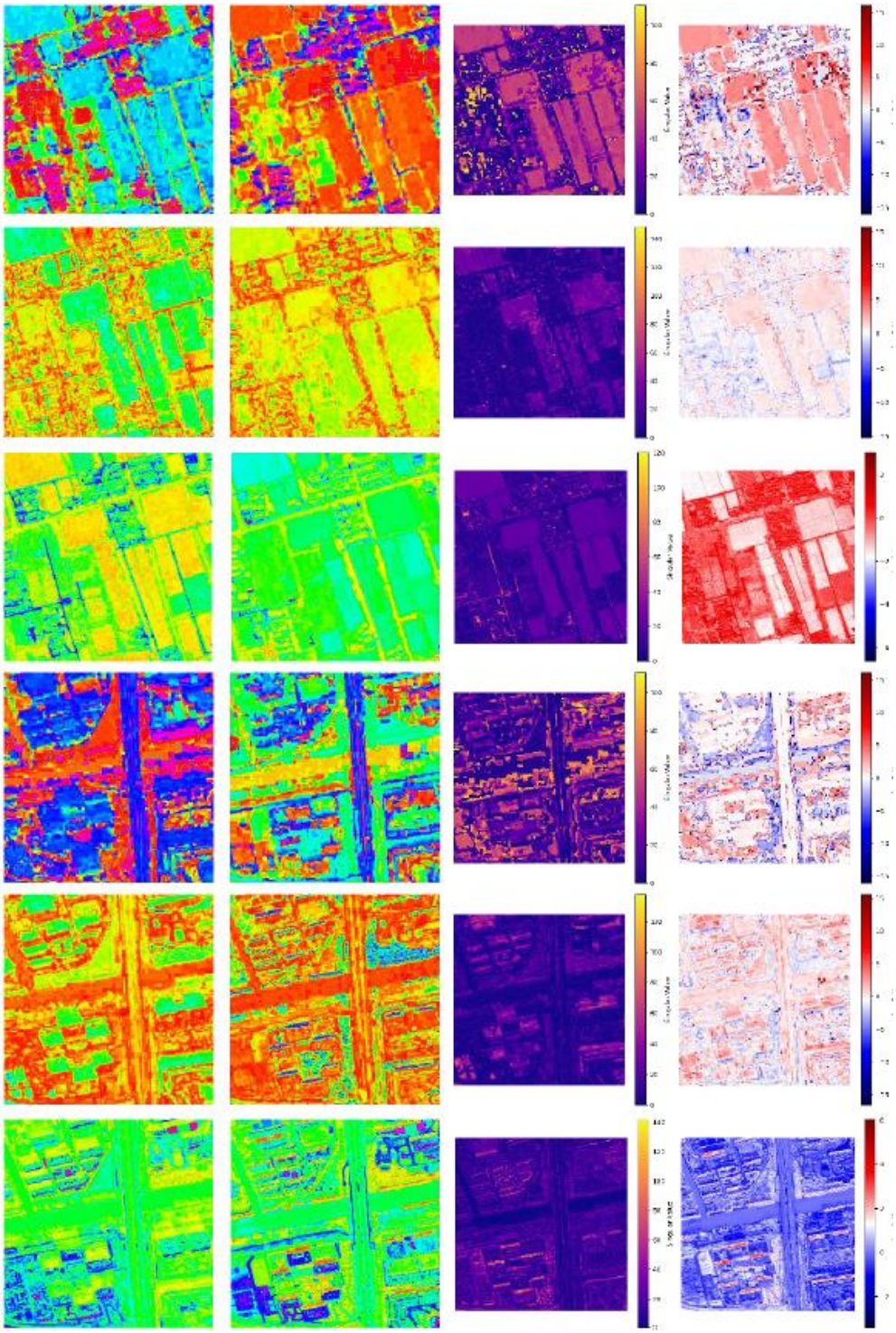

Figure 5. Data Train Processing Results

The resulting relationships are expressed in Equations 5 and 6.

$$\sigma_2 \geq \beta_1 \tag{5}$$

$$L_{Hue.Sat}(i,j) \geq \beta_2 \tag{6}$$

$$L_{Val}(i,j) \leq \beta_2$$

Equation 5 is derived from an analysis of Figure 5 in the section on singular value maps, which shows the distribution of the plotted results for the second singular value. The ≥ relationship in the equation is based on the observation that brighter pixel intensities indicate areas undergoing change, consistent with the color change indicator in the HSV channel. Brighter intensities indicate higher singular values, so this relationship can be formulated as Equation 5, with $\beta 1$ as the threshold to be determined in the next step. Equation 6 is derived from Figure 5 in the log-ratio map section, which illustrates the distribution of calculated log-ratio values. The formulation of this equation follows an approach similar to that for singular values, namely by utilizing brightness levels as an indicator of the intensity of change in pixels.

The thresholds $\beta 1$ and $\beta 2$ are determined by plotting the averages of all singular value maps and log ratio maps. Once the averages of all maps have been obtained, their mean is calculated again to serve as the threshold for each channel, with $\beta 1$ as the singular value threshold and $\beta 2$ as the log ratio threshold. The average plots are shown in Figure 6.

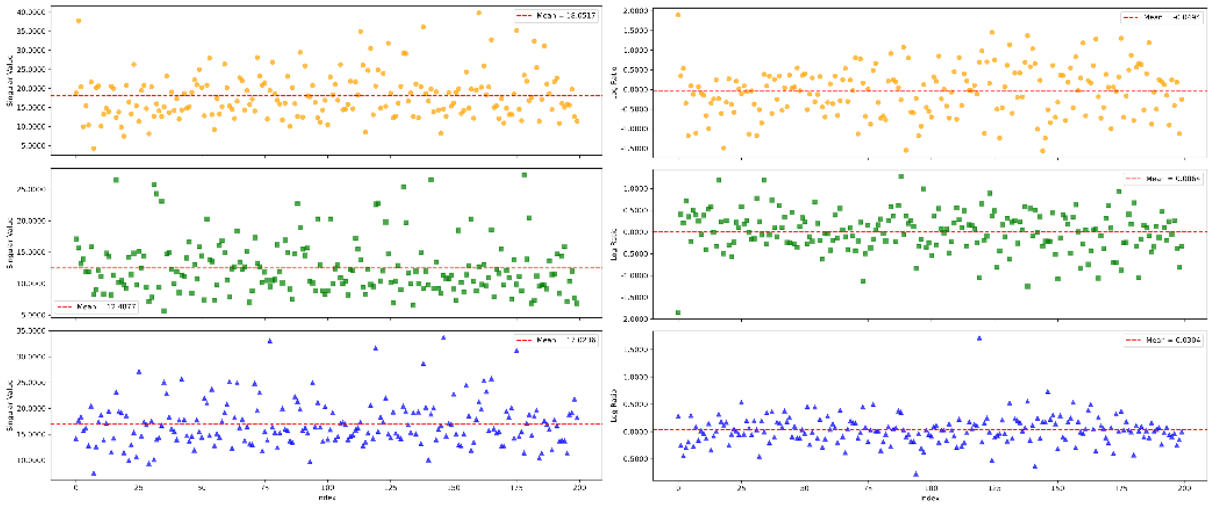

(a) (b)

Figure 6. Mean Plot of the Data Train Images; (a) Singular Value and (b) Log Ratio

In Figure 6, the yellow plot represents the hue channel, the green plot represents the saturation channel, and the blue plot represents the value channel. The red line running through the plots is the average line that will be used as the threshold. The thresholds obtained from Figure 6 are summarized in Table 2.

Tabel 2. β_1 and β_2 Results

Channel	β_1	β_2
Hue	18.0517	−0.0494
Saturation	12.4877	0.0064
Value	17.0236	0.0304

Next, $\beta 1$ and $\beta 2$, obtained in the previous step, serve as threshold conditions in the segmentation process using the SVD and log ratio approaches. The segmentation process is based on

comparing the singular values of the input images against $\beta 1$ and the log ratio values of the input images against $\beta 2$. Figure 7 shows a visualization of the segmentation results for each disaster dataset.

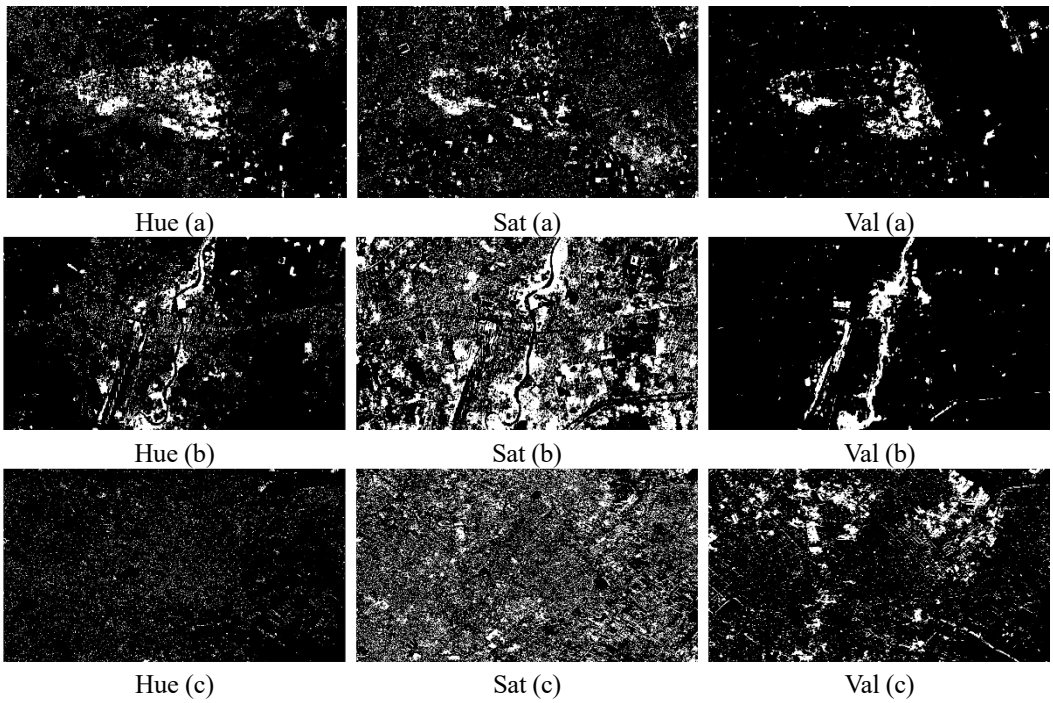

Figure 7. Segmentation Results for Each HSV Channel

Based on Figure 7, the first, second, and third disaster datasets are represented as points (a), (b), and (c), respectively. Visually, it appears that the saturation channel does not perform well with this algorithm. This is because, visually, the results from this channel appear to contain too much noise and over detection. Therefore, as part of the experiment, a better model will be developed. Visually, it can be observed that the Hue and Value channels tend to complement each other in disaster detection. The final result of the segmentation process is obtained by combining the three channels to achieve more accurate results, as shown in Figure 8.

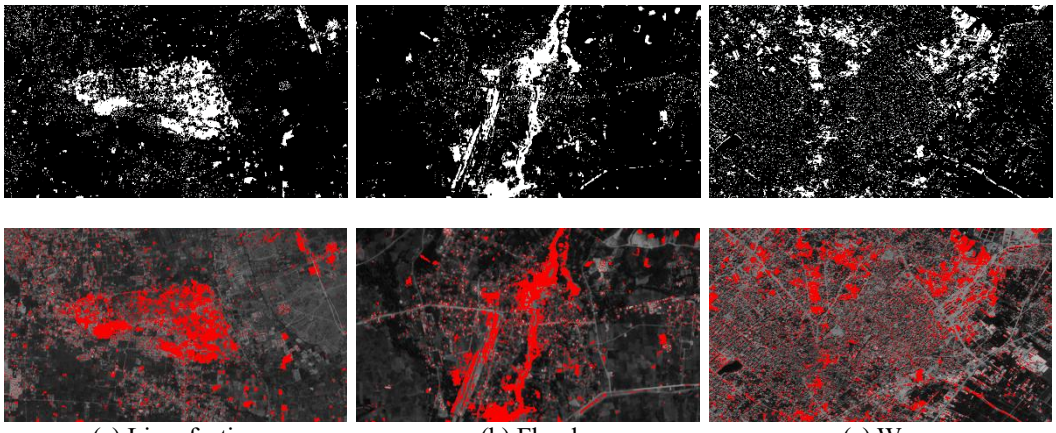

Figure 8. Final Segmentation Results

Based on Figure 8, the areas affected by the disaster can be visually identified. The red color in the figure indicates areas affected by the disaster. The affected areas are widely distributed across various regions, particularly in areas with open land and settlements in the case of liquefaction disasters. A more concentrated pattern of impact along major roads and in high-density urban areas is evident in the case of flood disasters. A more even distribution of impacts in urban areas, with a primary concentration around major road networks and activity centers, is shown for war disasters.

Table 3. Visual Comparison with Previous Methods

Data	**Segmentation Results**			
1	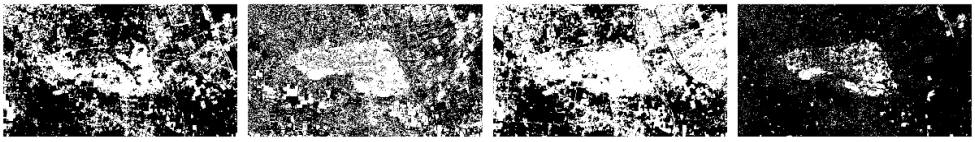			
2	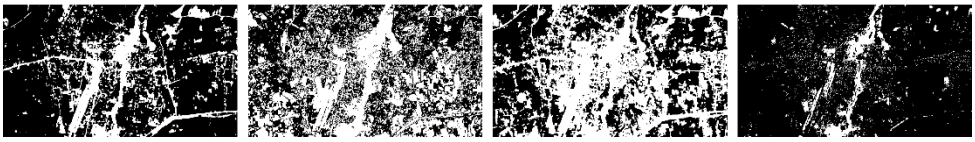			
3	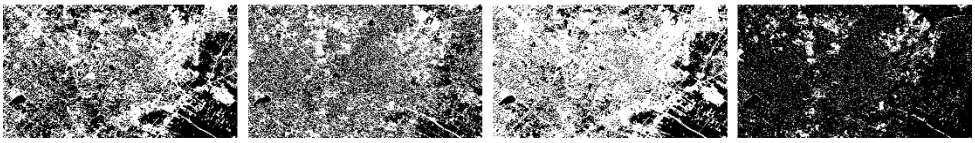			
Mtd.	Otsu	Region Growing	K-Means Clustering	Proposed
Ref.	[40]	[41]	[42]	Proposed

Table 3 presents the results of a comparison of segmentation using the Otsu, Region Growing, K-Means Clustering, and Proposed framework on three disaster datasets. The Otsu method produces high-contrast segmentation but lacks detail in areas of change. Region Growing provides more adaptive segmentation but is susceptible to variations in image intensity. K-Means Clustering is capable of grouping areas of change based on intensity similarity, but the results tend to lack precision in distinguishing object boundaries due to spectral variations within a single cluster. The proposed framework demonstrates clearer and more accurate segmentation results in detecting disaster-induced changes compared to the other methods. Quantitative evaluation was conducted by comparing the AUC values of each method to measure segmentation performance in detecting changes caused by disasters. Figure 9 displays the ROC curves for each method in the context of liquefaction (a), flooding (b), and war (c) as indicators of segmentation accuracy.

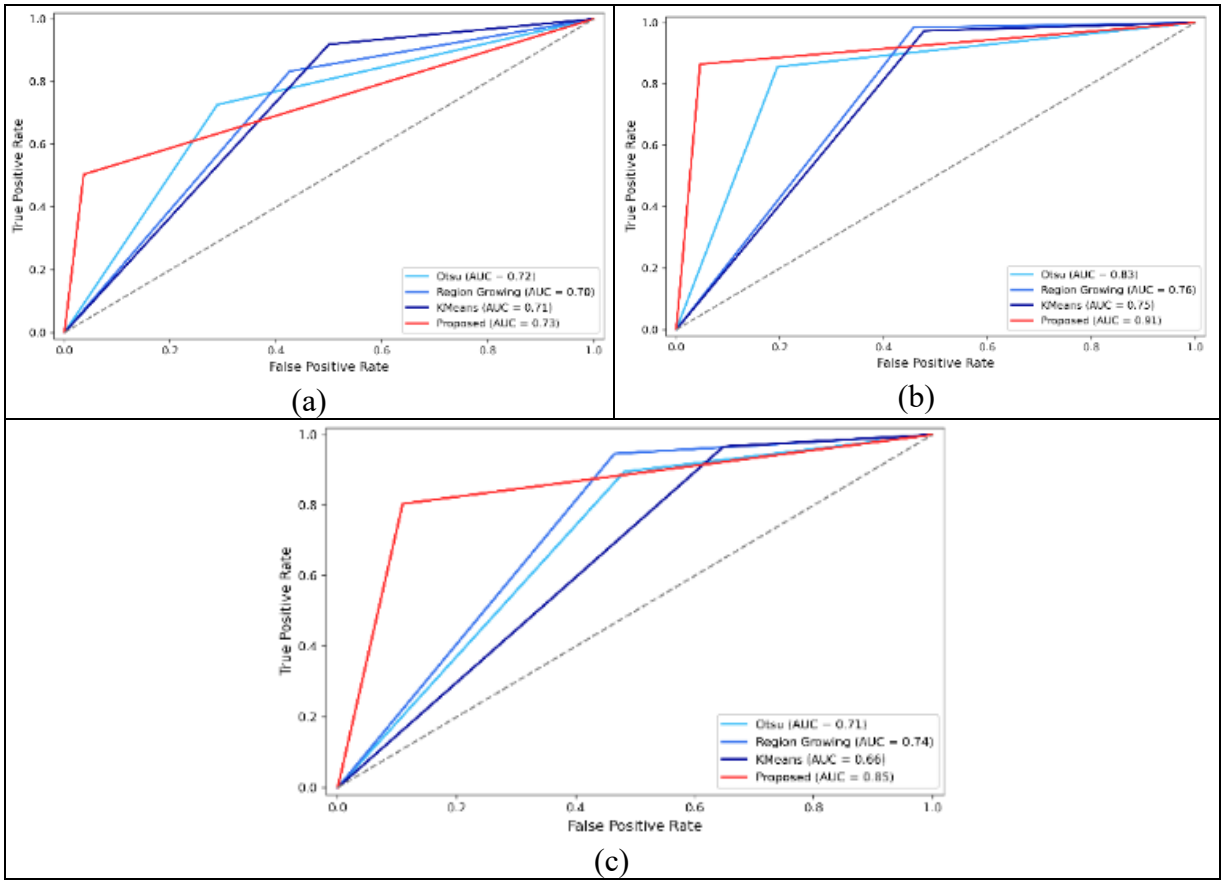

Gambar 9. ROC Curve and AUC Value for the Datatest

As shown in Figure 9, the ROC curve of the proposed framework generally exhibits a better pattern compared to the other methods. The curve of the combined method tends to be higher and further away from the diagonal line. The curves for the Otsu and Region Growing methods tend to follow a more stable pattern, while K-Means Clustering exhibits a more variable pattern. A quantitative comparison of the performance of each method is also presented through the AUC values calculated from the ROC curves in Table 4.

Table 4. Comparison by AUC Value

Data	Otsu Method	Region Growing	K-Means Clustering	Proposed Framework
1.	0.72	0.70	0.71	0.73
2.	0.83	0.76	0.75	0.91
3.	0.71	0.74	0.66	0.85
Ref	[40]	[41]	[42]	Proposed

Based on Table 4, the proposed combination method demonstrated the best performance compared to the other comparison methods. The AUC values obtained by the proposed framework were 0.73 for liquefaction data, 0.91 for flood data, and 0.85 for war data. The Otsu method achieved AUC values of 0.72, 0.83, and 0.71, respectively. The Region Growing method achieved AUC values of 0.70, 0.76, and 0.74. The K-Means Clustering method achieved AUC

values of 0.71, 0.75, and 0.66. Consistently higher AUC values indicate that the proposed method is superior in distinguishing affected and unaffected areas in satellite imagery [43].

IV. CONCLUSION

This study proposed a hybrid disaster damage segmentation framework that integrates Singular Value Decomposition (SVD) and Log-Ratio analysis for identifying disaster-affected areas from Sentinel-2 satellite imagery. The framework combines histogram matching and HSV color space transformation in the preprocessing stage, followed by local kernel-based singular value extraction and log-ratio computation to enhance change detection between pre-disaster and post-disaster images. Experimental results on liquefaction, flood, and war datasets demonstrated that the proposed method consistently outperformed conventional segmentation approaches, including Otsu Thresholding, Region Growing, and K-Means Clustering. The proposed framework achieved the highest segmentation performance with AUC values of 0.73, 0.91, and 0.85 for the three disaster scenarios, respectively. These findings indicate that the integration of singular value features and log-ratio analysis is effective in capturing subtle spatial changes while reducing the influence of intensity variations and noise. Furthermore, the generated disaster impact maps provide meaningful spatial information that can support rapid damage assessment, disaster response planning, and resilience-oriented decision-making in disaster-prone regions.

Future research should investigate the integration of the proposed SVD–Log Ratio framework with advanced machine learning and deep learning techniques to further improve segmentation accuracy and automation capabilities. The framework may also be extended to utilize multi-temporal and multi-sensor remote sensing data, such as Synthetic Aperture Radar (SAR) and high-resolution satellite imagery, to enhance robustness under diverse environmental conditions. In addition, future studies should evaluate the proposed method on larger and more diverse disaster datasets covering earthquakes, tsunamis, volcanic eruptions, and wildfires to assess its generalizability. The incorporation of real-time satellite data streams and cloud-based processing architectures could further support the development of operational disaster monitoring systems capable of providing timely information for disaster risk reduction, emergency management, and resilience planning.

V. AUTHOR CONTRIBUTION

The authors contributed equally to the formulation of the research concept, data collection, data analysis, manuscript writing, and approval of the final manuscript for publication.

VI. CONFLIC OF INTEREST

The authors declare that there are no potential conflicts of interest related to the research, writing, or publication of this article.

REFERENCES

[1] R. Cribb and M. Ford, "1 Indonesia as an Archipelago: Managing Islands, Managing the Seas," in *Indonesia beyond the Water's Edge*, ISEAS Publishing, 2009, pp. 1–27. doi: 10.1355/9789812309815-005.

[2] S. Munawaroh, "Penerapan sanksi penenggelaman kapal asing pelaku illegal fishing oleh pemerintah Indonesia (Perspektif hukum internasional)," *MIMBAR YUSTITIA*, vol. 3, no. 1, pp. 27–43, May 2019, doi: 10.52166/mimbar.v3i1.1739.

[3] A. White *et al.*, "Marine protected area networks in Indonesia: Progress, lessons and a network design case study covering six eastern provinces," *Coastal Management*, vol. 49, no. 6, pp. 575–597, Nov. 2021, doi: 10.1080/08920753.2021.1967560.

[4] M. P. Amarda and Syafriani, "Analysis of seismic hazards and vulnerability throughout Indonesia based on 1999-2003 earthquake data using the microseismic method," *PILLAR OF PHYSICS*, vol. 14, no. 2, Dec. 2021, doi: 10.24036/11929171074.

[5] P. A. Kaban, R. Kurniawan, R. E. Caraka, B. Pardamean, B. Yuniarto, and Sukim, "Biclustering method to capture the spatial pattern and to identify the causes of social vulnerability in Indonesia: A new recommendation for disaster mitigation policy," *Procedia Comput. Sci.*, vol. 157, pp. 31–37, 2019, doi: 10.1016/j.procs.2019.08.138.

[6] B. Kusumasari, "Natural Hazards Governance in Indonesia," in *Oxford Research Encyclopedia of Natural Hazard Science*, Oxford University PressNew York, NY, 2019. doi: 10.1093/acrefore/9780199389407.013.234.

[7] R. Djalante, "Identifying drivers, barriers and opportunities for integrating disaster risk reduction and climate change adaptation in Indonesia: An analysis based on the earth system governance framework," 2013, pp. 131–147. doi: 10.1007/978-3-642-31110-9_9.

[8] R. Djalante, "Research trends on hazards, disasters, risk reduction and climate change in Indonesia: A systematic literature review," May 11, 2016. doi: 10.5194/nhess-2016-112.

[9] R. Djalante, "Review article: A systematic literature review of research trends and authorships on natural hazards, disasters, risk reduction and climate change in Indonesia," *Natural Hazards and Earth System Sciences*, vol. 18, no. 6, pp. 1785–1810, Jun. 2018, doi: 10.5194/nhess-18-1785-2018.

[10] W. Mao and V. I. O. Agyapong, "The role of social determinants in mental health and resilience after disasters: Implications for public health policy and practice," *Front. Public Health*, vol. 9, May 2021, doi: 10.3389/fpubh.2021.658528.

[11] S. K. Patel, G. Agrawal, and B. Mathew, "Understanding the resilience and mental health impacts of natural disasters in India: A narrative review," *Int. J. Popul. Stud.*, vol. 6, no. 1, p. 82, Aug. 2024, doi: 10.18063/ijps.v6i1.1183.

[12] S. A. Saeed and S. P. Gargano, "Natural disasters and mental health," *International Review of Psychiatry*, vol. 34, no. 1, pp. 16–25, Jan. 2022, doi: 10.1080/09540261.2022.2037524.

[13] A. Bănică, K. Kourtit, and P. Nijkamp, "Natural disasters as a development opportunity: A spatial economic resilience interpretation," *Review of Regional Research*, vol. 40, no. 2, pp. 223–249, Oct. 2020, doi: 10.1007/s10037-020-00141-8.

[14] S. Lazzaroni and P. A. G. van Bergeijk, "Natural disasters' impact, factors of resilience and development: A meta-analysis of the macroeconomic literature," *Ecological Economics*, vol. 107, pp. 333–346, Nov. 2014, doi: 10.1016/j.ecolecon.2014.08.015.

[15] M. Y. Omelicheva, "Natural disasters: Triggers of political instability?," *International Interactions*, vol. 37, no. 4, pp. 441–465, Oct. 2011, doi: 10.1080/03050629.2011.622653.

[16] G. A. Arpitha, A. L. Choodarathnakara, A. Rajaneesh, G. S. Sinchana, and K. S. Sajinkumar, "Creation of a landslide inventory for the 2018 storm event of kodagu in the western ghats for landslide susceptibility mapping using machine learning," *Journal of the Indian Society of Remote Sensing*, vol. 52, no. 11, pp. 2443–2459, Nov. 2024, doi: 10.1007/s12524-024-01953-8.

[17] A. Balasundaram, A. B. Abdul Aziz, A. Gupta, A. Shaik, and M. S. Kavitha, "A fusion approach using GIS, green area detection, weather API and GPT for satellite image based fertile land discovery and crop suitability," *Sci. Rep.*, vol. 14, no. 1, p. 16241, Jul. 2024, doi: 10.1038/s41598-024-67070-1.

[18] S. Sadeghi, E. S. Teshnizi, R. R. Pash, and M. Golian, "Extraction of lineaments using landsat image and digital elevation model: A case study of zagros orogenic belt, West Iran," *Journal of the Indian Society of Remote Sensing*, vol. 52, no. 11, pp. 2361–2373, Nov. 2024, doi: 10.1007/s12524-024-01956-5.

[19] S. Zhang and J. Ma, "CascadeDumpNet: Enhancing open dumpsite detection through deep learning and AutoML integrated dual-stage approach using high-resolution satellite imagery," *Remote Sens. Environ.*, vol. 313, p. 114349, Nov. 2024, doi: 10.1016/j.rse.2024.114349.

[20] J. Doshi, S. Basu, and G. Pang, "From satellite imagery to disaster insights," Dec. 2018.

[21] B. K. Jones, T. S. Stryker, A. Mahmood, and G. R. Platzeck, "The international charter 'Space and major disasters,'" in *Time-Sensitive Remote Sensing*, New York, NY: Springer New York, 2015, pp. 79–89. doi: 10.1007/978-1-4939-2602-2_6.

[22] S. Liu and M. E. Hodgson, "Satellite image collection modeling for large area hazard emergency response," *ISPRS Journal of Photogrammetry and Remote Sensing*, vol. 118, pp. 13–21, Aug. 2016, doi: 10.1016/j.isprsjprs.2016.04.007.

[23] F. Gouveia, V. Silva, J. Lopes, R. S. Moreira, J. M. Torres, and M. Simas Guerreiro, "Automated identification of building features with deep learning for risk analysis," *Discover Applied Sciences*, vol. 6, no. 9, p. 466, Aug. 2024, doi: 10.1007/s42452-024-06070-2.

[24] Z. Su *et al.*, "A new and robust index for water body extraction from sentinel-2 imagery," *Remote Sens. (Basel).*, vol. 16, no. 15, p. 2749, Jul. 2024, doi: 10.3390/rs16152749.

[25] B. Wu, Y. Wang, H. Huang, S. Liu, and B. Yu, "Potential of SDGSAT-1 nighttime light data in extracting urban main roads," *Remote Sens. Environ.*, vol. 315, p. 114448, Dec. 2024, doi: 10.1016/j.rse.2024.114448.

[26] S. Cottrell, R. Wang, and G.-W. Wei, "PLPCA: Persistent laplacian-enhanced PCA for microarray data analysis," *J. Chem. Inf. Model.*, vol. 64, no. 7, pp. 2405–2420, Apr. 2024, doi: 10.1021/acs.jcim.3c01023.

[27] S. Duan, J. Yang, X. Han, and G. Liu, "Adaptive dimensionality reduction method for high-dimensional data," *Journal of Mechanical Engineering*, vol. 60, no. 17, p. 283, 2024, doi: 10.3901/JME.2024.17.283.

[28] R. A. Kolajoobi, C. MacBeth, and J. Landa, "Improving 4D seismic history matching through data analysis: A localized sensitivity analysis workflow," *SPE Journal*, vol. 29, no. 09, pp. 4815–4826, Sep. 2024, doi: 10.2118/221467-PA.

[29] F. Rajabi and J. J. McArthur, "Applying OPTICS with and without PCA for fault detection of fan coil units using building automation system data," *Energy Build.*, vol. 317, p. 114368, Aug. 2024, doi: 10.1016/j.enbuild.2024.114368.

[30] A. Abdurrazzaq, A. K. Junoh, Z. Yahya, and I. Mohd, "New white blood cell detection technique by using singular value decomposition concept," *Multimed. Tools Appl.*, vol. 80, no. 3, pp. 4627–4638, Jan. 2021, doi: 10.1007/s11042-020-09946-8.

[31] S. D'Iorio, L. Forzani, R. García Arancibia, and I. Girela, "Predictive power of composite socioeconomic indices for targeted programs: Principal components and partial least squares," *Qual. Quant.*, vol. 58, no. 4, pp. 3497–3534, Aug. 2024, doi: 10.1007/s11135-023-01811-8.

[32] H. Wang, J. Shi, Y. Yang, K. Ma, and Y. Xue, "Machine learning methods predict recurrence of pN3b gastric cancer after radical resection," *Transl. Cancer Res.*, vol. 13, no. 3, pp. 1519–1532, Mar. 2024, doi: 10.21037/tcr-23-1367.

[33] T. Yan, Y. Wang, and P. Wang, "Rational polynomial coefficient estimation via adaptive sparse PCA-based method," *Remote Sens. (Basel).*, vol. 16, no. 16, p. 3018, Aug. 2024, doi: 10.3390/rs16163018.

[34] X. Hu, C. V. Tao, and B. Prenzel, "Automatic segmentation of high-resolution satellite imagery by integrating texture, intensity, and color features," *Photogramm. Eng. Remote Sensing*, vol. 71, no. 12, pp. 1399–1406, Dec. 2005, doi: 10.14358/PERS.71.12.1399.

[35] Z. Hu, Z. Wu, Q. Zhang, Q. Fan, and J. Xu, "A spatially-constrained color–texture model for hierarchical VHR image segmentation," *IEEE Geoscience and Remote Sensing Letters*, vol. 10, no. 1, pp. 120–124, Jan. 2013, doi: 10.1109/LGRS.2012.2194693.

[36] T. Sai Kumar, M. Chandra M, and S. Murthy P, "Colour-based image segmentation using fuzzy C-Means clustering," *International Journal on Intelligent Electronic Systems*, vol. 5, no. 2, pp. 47–51, 2011, doi: 10.18000/ijies.30099.

[37] S. Liu, Z. Cao, and J. Li, "A SVD-based visual attention detection algorithm of SAR image," in *Lecture Notes in Electrical Engineering*, 2014. doi: 10.1007/978-3-319-00536-2_55.

[38] Copernicus Browser, "Copernicus Open Access Hub." [Online]. Available: https://browser.dataspace.copernicus.eu/

[39] K. Yang *et al.*, "Semantic change detection with asymmetric siamese networks," May 2021.

[40] Y. Du, H. Yuan, K. Jia, and F. Li, "Research on threshold segmentation method of two-dimensional otsu image based on improved sparrow search algorithm," *IEEE Access*, vol. 11, pp. 70459–70469, 2023, doi: 10.1109/ACCESS.2023.3293191.

[41] G. Surówka and M. Ogorzałek, "Segmentation of the melanoma lesion and its border," *International Journal of Applied Mathematics and Computer Science*, vol. 32, no. 4, 2022, doi: 10.34768/amcs-2022-0047.

[42] D. G. Olle, J. Z. Bisse, and G. A. Alo'o, "Application and comparison of K-means and PCA based segmentation models for Alzheimer disease detection using MRI," *Discover Artificial Intelligence*, vol. 4, no. 1, p. 11, Feb. 2024, doi: 10.1007/s44163-024-00106-7.

[43] L. Carrington, L. Hale, C. Freeman, D. Smith, and M. Perry, "The effectiveness of play as an intervention using International classification of functioning outcome measures for children with disabilities – a systematic review and meta-synthesis," *Disabil. Rehabil.*, vol. 46, no. 17, pp. 3827–3848, Aug. 2024, doi: 10.1080/09638288.2023.2259305.